Journal of Materials Chemistry

Dynamic Article Links

Cite this: *J. Mater. Chem.*, 2011, **21**, 6020

www.rsc.org/materials

PAPER

An all-inorganic type-II heterojunction array with nearly full solar spectral response based on ZnO/ZnSe core/shell nanowires

Zhiming Wu,*[a] Yong Zhang,[b] Jinjian Zheng,[a] Xiangan Lin,[a] Xiaohang Chen,[a] Binwang Huang,[a] Huiqiong Wang,[a] Kai Huang,[a] Shuping Li[a] and Junyong Kang*[a]

Received 18th November 2010, Accepted 16th February 2011
DOI: 10.1039/c0jm03971c

Well-aligned ZnO/ZnSe core/shell nanowire arrays with type-II energy alignment are synthesized *via* a two-step chemical vapor deposition method. Morphology and structure studies reveal a transition layer of wurtzite ZnSe between the wurtzite ZnO core and the cubic ZnSe shell. Type-II interfacial transitions are observed in the spectral region from visible to near infrared in transmission and photoluminescence. More significantly, for the first time, the interfacial transition is shown to extend the photoresponse of the prototype photovoltaic device based on the coaxial nanowire array to a threshold much below the bandgap of either component (3.3 and 2.7 eV, respectively) at 1.6 eV, with an external quantum efficiency of ~4% at 1.9 eV and 9.5% at 3 eV. These results represent a major advance towards the realization of all-inorganic type-II heterojunction photovoltaic devices in an optimal device architecture.

1. Introduction

Solar cells have been a subject of great interest due to the growing awareness of energy shortage and environmental protection.[1–4] Various photovoltaic devices have been developed based on inorganic or organic materials, such as silicon-based thin film solar cells,[2] multi-junction solar cells,[3] and dye-sensitized solar cells (DSSCs).[4] Nevertheless, most of them suffer from either high cost or relatively low energy conversion efficiency. The use of nanostructured materials, especially nanowire arrays (NWAs), is deemed as one of the promising approaches to overcome these issues.[5–10] Nanowires have been suggested to be superior to the bulk or film materials in both surface-to-volume ratio and crystalline quality, leading to an increase of junction areas and a reduction of defect recombination of photogenerated carriers. In addition, NWAs can effectively reduce light loss through the increase of light coupling and decrease of reflectance.[11,12] Furthermore, recent theoretical studies reveal that coaxial nanowires can further enhance carrier collection because of the novel mechanism of radial charge separation.[13–16] In light of these advantages, various types of coaxial NWAs based on either homostructure or heterostructure materials have been proposed or developed for the applications in photovoltaic devices.[17–25]

ZnO NWAs have been widely synthesized and used in the photovoltaic devices due to their stability and non-toxicity as well as relatively mature growth techniques,[26,27] such as chemical vapor deposition method, Sol–Gel method, and electrochemical deposition method. It was typically used as a transparent conductive electrode or carrier transporter in "sensitized" solar cells utilizing its large bandgap. Recently, ZnO has been proposed to form type-II heterojunctions with other wide bandgap II–VI semiconductors, such as ZnSe, ZnS, and ZnTe,[10,22–24,28] as an alternative structure for photovoltaic applications.[14,16] These wide bandgap materials alone can not absorb the sun light efficiently. Nevertheless, it has been predicted that if two large bandgap materials with type-II band alignment form coaxial nanowires, the effective indirect bandgap could be substantially smaller than either of the individual materials.[14,16] As a result, the absorption threshold could be extended to a significantly longer wavelength by interfacial transitions. However, the predicted extension to the longer wavelength well beyond that set by the lower-bandgap has not yet been convincingly realized.[22–24] Particularly, ZnO/ZnSe core/shell nanowire arrays have been predicted to exhibit large band offsets to confine carriers and thus explored experimentally for this purpose.[22] It is a great challenge to obtain good crystalline quality of the core-shell structure. Therefore, it is crucially important to control the nanowire size and the growth conditions in order to further explore this unconventional approach.

The idea of constructing a photovoltaic device using the type-II heterostructure instead of the p–n junction has been developed with great success in organic PV–bulk heterojunction solar cells and dye-sensitized solar cells. The development of an

[a]*Fujian Key Laboratory of Semiconductor Materials and Applications, Department of Physics, Xiamen University, Xiamen, 361005, P. R. China. E-mail: zmwu@xmu.edu.cn; jykang@xmu.edu.cn*
[b]*Department of Electrical and Computer Engineering and Center for Optoelectronics, University of North Carolina at Charlotte, Charlotte, NC, 28223, USA*

all-inorganic version has two major advantages: (1) it provides an improved chemical stability of the material and the device, and (2) it allows the realization of an interfacial absorption that is typically very weak for the organic materials. Furthermore, even within the inorganic options, the large bandgap materials like ZnO and ZnSe are known to be much more stable than others such as CdTe.

In this work, we have successfully synthesized type-II ZnO/ZnSe core/shell NWAs with wurtzite ZnSe transition layer on a large-area transparent quartz glass using a two-step chemical vapor deposition (CVD) method. The morphologies, structural properties and the chemical compositions of ZnO/ZnSe core/shell nanowires were characterized by scanning electron microscopy (SEM), X-ray diffraction (XRD), and energy-dispersive X-ray spectroscopy (EDS), respectively. The heterojunction interface was investigated by high-resolution transmission electron microscopy (HR-TEM). The type-II interfacial transitions in coaxial nanowires were analyzed by optical transmission and photoluminescence (PL). A prototype photovoltaic device based on the ZnO/ZnSe core/shell NWAs was fabricated. The photoresponse was measured by using a broadband spectroscopy system.

2. Experiment

The growth of well-aligned ZnO NWAs was carried out in a horizontal quartz tube furnace with three heating zones. High purity metallic zinc powder (5N, 3.0 g) was used as the source material and placed at the central heating zone. Prior to ZnO nanowire growth, a 1 μm thick ZnO film was deposited on the quartz glass substrate by molecular beam epitaxy (MBE) at room temperature. The substrate with the dimension of 1.5 cm × 1.5 cm was placed at the central zone downstream of the Zn powder at a distance of 7 cm. Before heating, the system was evacuated to 1.0×10^{-2} Pa, and a mixed gas consisting of 200 sccm N_2 flow and 10 sccm O_2 flow was introduced into the tube (sccm: standard cubic centimetre per minute). Then, the tube was heated to 600 °C at a rate of 20 °C/min and kept at this temperature for 30 min. To grow the ZnSe shell outside the ZnO nanowires, high purity Se powder (5N, 0.2g) was placed at the first zone upstream of the Zn power after the tube furnace was cooled down to room temperature. Subsequently, the system was evacuated again and only 200 sccm N_2 flow passed through the tube as the carrier gas. The heating zones were heated at a rate of 10 °C/min. During the ZnSe shell growth, the temperature of the central zone was kept at 620 °C while the first zone was controlled at 420 °C. After 120 min growth, the system was naturally cooled down to room temperature.

Morphologies of the as-grown ZnO and ZnO/ZnSe NWAs were characterized by a field emission SEM (FE-SEM, LEO 1530). The structures and compositions were analyzed by XRD (Oxford Gemini SUltra) using the grazing angle (5°) mode, as well as TEM (Tecnai F30), and EDS. An ultraviolet visible spectrophotometer (Varian Cary 100) was used to measure the transmission spectra for different samples. Additionally, PL spectra were measured at room temperature using a KrF excimer laser (248 nm) as an excitation source and a fiber optic spectrometer (AvaSpec-ULS2048), which consists of a CCD detector with 2048 pixels.

To investigate the photoresponse of the ZnO/ZnSe core/shell NWA, the nanowire wafer was bonded with a 200 nm thick indium tin oxide (ITO) film deposited on the quartz glass, and the ZnO thin film was contacted with an indium probe. The device structure is shown schematically in Fig. 1. The effective device area is about 1.0 cm^2. The external quantum efficiency (EQE) was measured on a broadband spectroscopy system consisting of a grating monochromator (Acton Research Corporation, SpectraPro-750i), a 200 W bromine-tungsten lamp, and a locked-in amplifier (Stanford Research Systems, SR830 DSP), by comparing with a reference Si cell (calibrated by Newport, 66902-QE). To further study the photoresponse of photovoltaic device, the open-circuit voltage of the device was measured under the radiation source of a red LED light or indoor sunlight. The power density of the radiation sources were both measured to be 50 μW/cm^2 by using a spectroradiometer (Spectro 320 optical scanning spectrometer). In addition, a defocused 10 mW He–Ne laser was used to measure the dependence of the photovoltage on the power density for the prototype photovoltaic device and the reference Si cell (with an energy conversion efficiency of 12.5% under one-sun). The red LED light had a main emission peak at 1.97 eV and a full width at half maximum of 0.05 eV, the sun light had a broad spectrum ranging from 0.6 to 4.0 eV, while the He–Ne laser had a sharp emission peak at 1.96 eV.

3. Results and discussion

The morphologies of the as-grown ZnO NWA and ZnO/ZnSe core/shell NWA were characterized by SEM. As shown in Fig. 2 (a), well-aligned ZnO nanowires with a length of about 1.4 μm were grown vertically from the ZnO film substrate. The nanowires have a hexagonal end plane, as shown in the inset of Fig. 2 (a), demonstrating the [0001] growth direction. In addition, benefiting from the self-catalyzed growth mechanism, nanowires have a smooth lateral surface and uniform diameter along their entire length. These structural properties qualitatively favor the formation of heterojunction with an abrupt interface. Moreover, the appropriate density and diameter of ZnO nanowires are very crucial to deposit high quality ZnSe shell. If the density is too high and/or the diameter is too large, it would be difficult to deposit the ZnSe shell layer surrounding the entire ZnO nanowire.[29] For low density and/or small diameter of ZnO nanowires, the deposition of ZnSe shell layer becomes easier, but such a structure reduces light absorption areas and thus degrades the

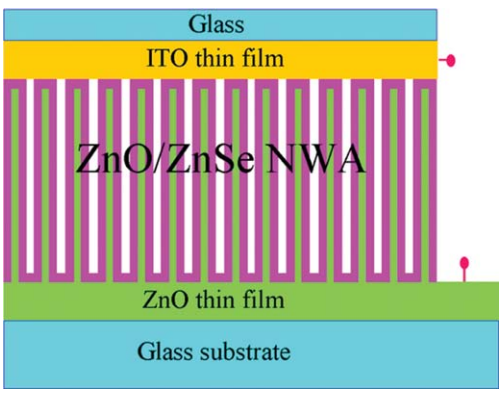

Fig. 1 Sketch of a ZnO/ZnSe NWA prototype photovoltaic device.

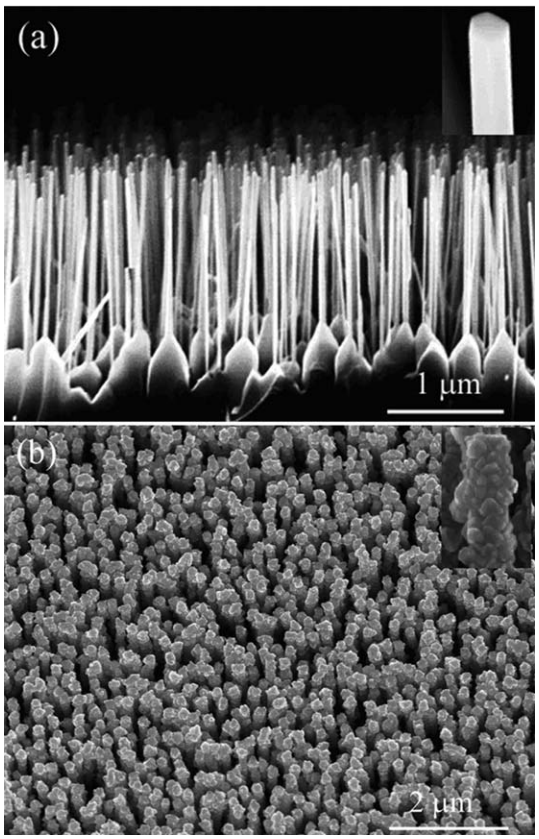

Fig. 2 SEM images of (a) well-aligned ZnO NWA and (b) well-aligned ZnO/ZnSe core/shell NWA. The insets in (a) and (b) are high-magnification SEM images of a single ZnO and a ZnO/ZnSe core/shell nanowire, respectively.

photoelectric conversion efficiency despite of the easiness of coating ZnSe shell. In our work, ZnO film with tapered grains of about 250 nm was grown *via* modifying the growth temperature. The ZnO nanowires prefer to grow on the top of ZnO (0001) grains due to their lowest surface energy, and their diameters are determined by the top surface size of grains, varying from 40 to 80 nm. Fig. 2(b) shows an image of ZnO/ZnSe core/shell NWA. The ZnO/ZnSe nanowires exhibit a larger diameter and rougher surface, compared to those ZnO nanowires, indicating the formation of core/shell structure. The ZnSe shells have roughly the same thickness, and almost all the nanowires are coated. This ensures a large surface-to-volume ratio of the core/shell heterostructures for a high absorption and conversion efficiency. Additionally, the ZnO/ZnSe core/shell nanowires are almost of the same height, which makes it possible to fabricate the contact of most of core/shell nanowires to the ITO electrode in the bonding process, and therefore ensures its feasibility in the photovoltaic device.

The structures of ZnO and ZnO/ZnSe NWAs were determined by XRD. For the ZnO NWA, only a strong peak is exhibited at 34.48°, indexed as (002) of wurtzite (WZ) ZnO, as shown in Fig. 3 (a). The sharp (002) peak confirms that ZnO nanowires have grown along their *c*-axis perpendicular to the substrate with good crystalline quality. Besides this ZnO peak, as shown in Fig. 3(b), three additional peaks at 27.18°, 45.20°, and 53.53° appear in the XRD patterns of the ZnO/ZnSe coaxial nanowires, which can be

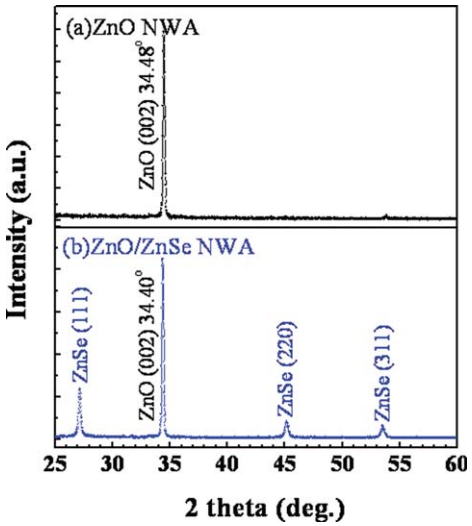

Fig. 3 XRD patterns of (a) ZnO NWA and (b) ZnO/ZnSe core/shell NWA.

assigned to zinc blende (ZB) phase ZnSe (111), (220), and (311) peaks, respectively. Interestingly, the ZnO (002) peak slightly shifts to the smaller angle of 34.40°, suggesting that the lattice of the core may suffer a tensile strain.[22] This behavior can be attributed to the fact that the ZnO core has a much smaller lattice constant than the ZnSe shell.

The microscopic structures of the ZnO/ZnSe core/shell nanowire were further characterized by TEM. Fig. 4(a) shows a low-magnification TEM image of a ZnO/ZnSe core/shell nanowire. A clear interface appears between the homogeneous ZnO core and rough ZnSe shell, confirming the formation of the core/shell structure. Meanwhile, it can be seen that the ZnSe shell is deposited over the entire ZnO nanowire, suggesting that the whole nanowire surface can be functionalized in the process of charge separation. There is a brighter contrast layer with thickness varying from 2 to 12 nm in the interface region. This typically arises from different materials or different phases in TEM imaging. To determine the concrete compositions, EDS line-scan of the elements were performed across the nanowire. As shown in the profiles of Fig. 4(b), the EDS spectra contain only three characteristic peaks of Zn, Se, and O elements. The Zn element appears in both the core and shell region, and the shoulder shape reveals the difference between the element in the core and that in the shell, supporting the contrast in the TEM image. And as expected, there are two Se peaks displaying in the shell regions, confirming the formation of ZnSe compounds, and the O element only appears in the core region. Interestingly, as shown in Fig. 4(b), the transition layer shows a low contrast in the dark field image, corresponding to the dip of the Zn curve at the interface, which indicates the existence of a new structure. To clarify this structure, the transition layer between WZ ZnO core and ZB ZnSe shell was further characterized by HR-TEM. As shown in Fig. 4(c), the top right corner exhibits a lattice fringe spacing of 0.260 nm, corresponding to WZ ZnO core with [0001] growth direction, whereas the lower left corner shows a spacing of 0.327 nm, corresponding to ZB ZnSe shell along the [111] direction. The middle region with brighter contrast is allocated to the transition layer. An abrupt interface appears between the

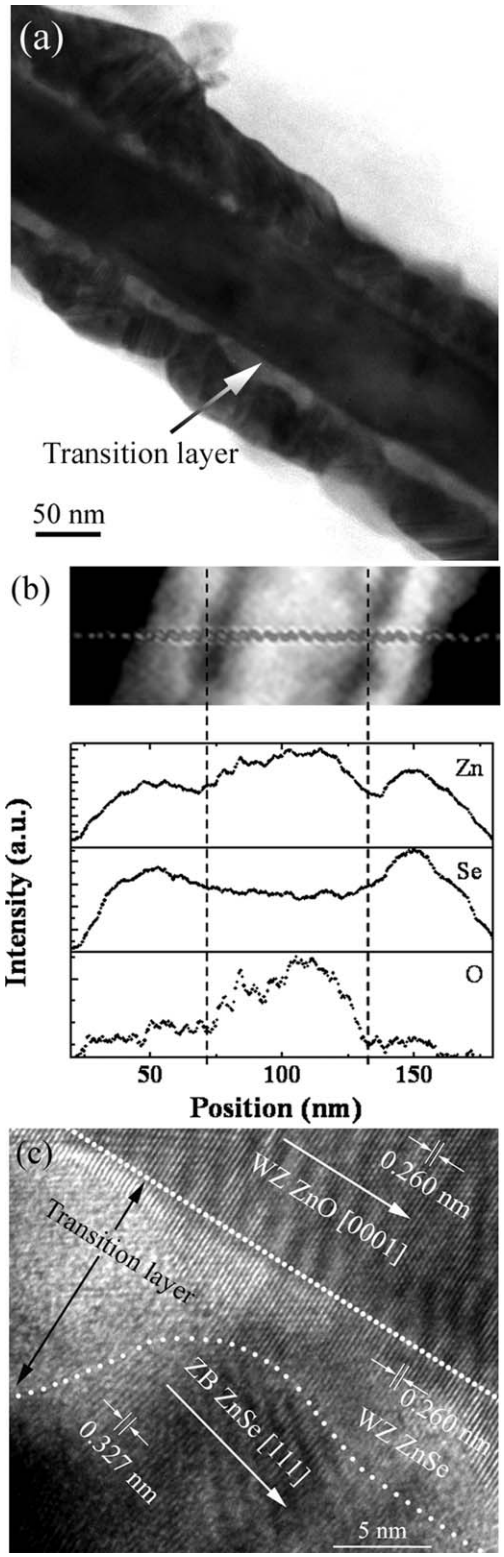

Fig. 4 (a) Low-magnification TEM image of a ZnO/ZnSe core/shell nanowire. (b) EDS line-scan profiles of the elements Zn, Se, and O across a ZnO/ZnSe core/shell nanowire. (c) High-resolution TEM image of the interface between the ZnO core and the ZnSe shell.

ZnO core and transition layer due to the smooth ZnO lateral surface, as marked by a dotted line. There is an irregular boundary between the transition layer and ZB ZnSe shell, resulting in the inhomogeneous thickness of the transition layer. Notably, the ZnSe transition layer grew coherently and laterally on the WZ ZnO and showed the same lattice constants of $a = 0.325$ and $c = 0.520$ nm as those of ZnO core. However, these values are smaller than those of bulk WZ ZnSe reported in the literature ($a = 0.3996$ nm and $c = 0.6550$ nm, JCPDS Card No. 15-0105). Hence, this WZ ZnSe transition layer is subjected to a compressive strain, whereas, the ZnO core is under a tensile strain, resulting in the XRD peak shift towards the smaller angle as demonstrated in Fig. 3. The coherent growth of WZ ZnSe could be attributed to the low-temperature growth stage during the ramping process.[30] The lack of an apparent XRD peak for this WZ ZnSe material is due to the overshadow of the strong WZ ZnO peak at almost the same position. The observed core/shell structure here is very different from what reported previously in which the ZnSe shell was found in the ZB phase with the [001] axis matching the c axis of ZnO.[22] The appearance of the transition layer represents the formation of a new ZnO/ZnSe core/shell structure, and might result in novel optical properties.

The electronic structures of the ZnO and ZnO/ZnSe core/shell NWA were investigated by transmission and PL measurements. Fig. 5(a) and (b) show the transmission spectra of ZnO and ZnO/ZnSe core/shell NWA and their derivative curves, respectively. For the ZnO NWA, only one distinct peak is observed at about 3.2 eV, which arises from the ZnO near-band-edge (NBE) absorption. For the ZnO/ZnSe core/shell NWA, three distinct absorption peaks are observed in Fig. 5(b). Besides the absorption in region II attributing to ZB ZnSe NBE absorption, the

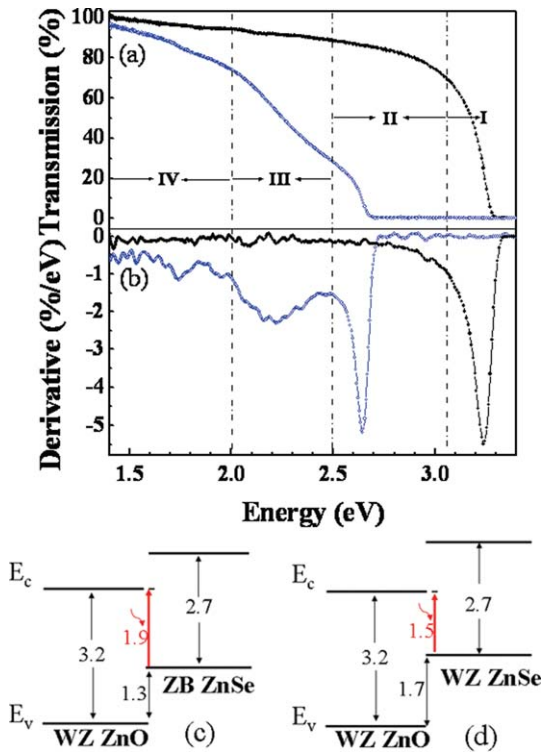

Fig. 5 (a) Transmission spectra of ZnO NWA (solid circle) and ZnO/ZnSe core/shell NWA (open circle) together with the substrate. (b) Derivative curves of the transmission spectra (a). Energy band diagrams for (c) WZ ZnO and ZB ZnSe heterojunction and (d) WZ ZnO and WZ ZnSe heterojunction.

absorption in regions III and IV are found to extend from visible to near infrared light. To clarify the origins of the absorption in region III and IV, we calculated the energy band structures at the interface of coaxial nanowires using Vienna Ab initio Simulation Package (VASP) based on the first-principles density functional theory (DFT).[31–34] The interface models between WZ ZnO and ZB ZnSe and that between WZ ZnO and WZ ZnSe were constructed, respectively. The calculations show that both WZ ZnO/ZB ZnSe and WZ ZnO/WZ ZnSe interfaces form type-II energy alignments with a band offset of 1.3 and 1.7 eV, respectively, as shown in Fig. 5(c) and (d). The absorption in region III may arise from the interfacial transition between WZ ZnO and ZB ZnSe (Fig. 5(c)). In addition, the absorption in the region IV from red to infrared spectral range is attributed to the interfacial transition between WZ ZnO and WZ ZnSe (Fig. 5(d)). Therefore, the transition at the type-II interface between the ZnO core and WZ ZnSe layer is responsible for the extension of the absorption energy to near infrared, which is important for photovoltaic applications.

Fig. 6 shows the normalized PL spectra for ZnO NWA and ZnO/ZnSe core/shell NWA. There is only one strong NBE emission of ZnO nanowires observed at 3.17 eV for ZnO NWA, indicating low defect density. This emission becomes very weak in the ZnO/ZnSe core/shell NWA. Instead, a distinct peak emerges in the region from 1.7 to 2.0 eV, corresponding to the near infrared absorption in Fig. 5. There could be several possible origins for this emission, such as interfacial transitions and defect-related recombination in nanowires. The defect-related emission in ZnO nanowires typically exhibits a broad band in the green or yellow spectral range,[22,35,36] which is very different from our PL spectrum that shows a sharp peak at 1.9 eV with a full width at half maximum of 0.14 eV. Additionally, as seen in Fig. 4(a) and (c), a thin coherent WZ ZnSe transition layer appears between the WZ ZnO core and ZB ZnSe shell, indicating a relatively good crystalline quality at the interface. Hence, the emission is more likely due to the interfacial transition rather than the defect recombination. The weakening of the ZnO NBE emission can be caused by the following three possible reasons: (1) charge separation between the core and shell by type-II energy alignment, resulting in a low hole concentration and recombination rate in ZnO core; (2) absorption of ZnSe shell and the emission of lower energy photons below the bandgap of ZnO or ZnSe, and (3) non-radiative recombination due to the interfacial defects. Since the emission related to ZnSe shell is weak as well and the interfacial emission is relative strong, the charge separation is expected to be quite efficient. It can thus be concluded that the type-II band alignment for the ZnO/ZnSe core/shell nanowires can efficiently separate photogenerated carriers, which will be further unambiguously supported by the photoresponse measurement described below.

Fig. 7 shows the EQE of the coaxial nanowire cell as a function of the light wavelength. A strong photoresponse band emerges in the energy range well below the bandgap of ZnSe, with the peak energy at ~1.9 eV and a threshold at as low as 1.6 eV. The EQE in the red spectral range reaches about 4% at 1.9 eV, which is comparable to the maximum of about 9.5% at 3 eV. The long wavelength response can be explained as the result of the type-II interfacial transition, although the detailed underlying physics required further investigation. The strong near-infrared response indicates rather efficient interfacial absorption in the core/shell NWA, due to two mechanisms (1) the light trapping effect and (2) the wave function overlap between the conduction band of ZnO core and valence band of ZnSe layer as a result of quantum confinement effect.[37] The low threshold can be attributed to the interfacial transition between the ZnO core and WZ ZnSe layer. When the photovoltaic device was irradiated by the red LED light with a power density of 50 $\mu W/cm^2$, the open-circuit voltage was determined to be 120 mV; whereas the open-circuit voltage increased to 320 mV when the indoor sunlight with the same power density was used. These results not only further confirm the strong photoresponse by interfacial transitions for the prototype device, but also indicate its potential as a high-efficiency cell with nearly full solar spectral response.

We have further investigated the dependence of open-circuit voltage V_{oc} on power density for the photovoltaic device as well as a reference Si cell using a He–Ne laser that outputs 10 mW at 632.8 nm (1.96 eV), with the results shown in Fig. 8. To ensure the uniform irradiation on the device, we defocused the laser spot to an area of approximately 1 cm^2. As expected, the open-circuit voltage increases with power density for both cells. However, the

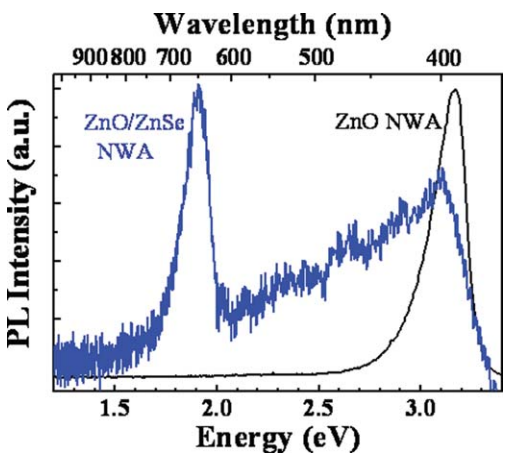

Fig. 6 Normalized PL spectra for ZnO NWA and ZnO/ZnSe core/shell NWA.

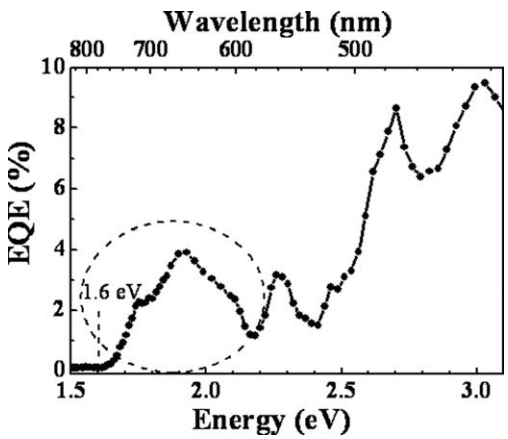

Fig. 7 EQE of a photovoltaic device based on the ZnO/ZnSe core/shell NWA.

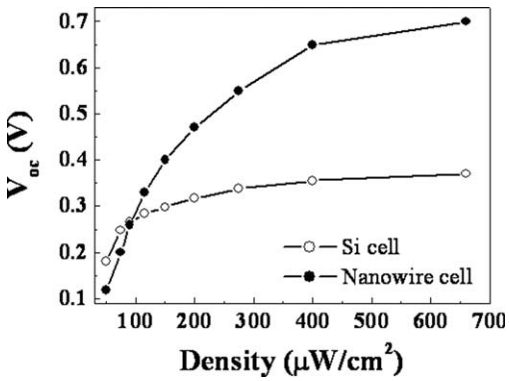

Fig. 8 Open-circuit voltage of the NWA cell and Si cell radiated by a He–Ne laser with different power densities.

V_{oc} for the NWA cell becomes larger than that of Si cell when the radiation density exceeds 100 μW/cm^2, and reaches 0.70 V under the highest available radiation density of 660 μW/cm^2, much higher than the value of 0.37 V from the Si cell, which further confirms the strong response in the red region due to the presence of interfacial transitions. The observed 0.70 V V_{oc} is among the highest reported values for the nanowire based solar cells.[38] The behavior of the Si cell is typical for a p–n junction solar cell where V_{oc} depends weakly on the radiation density. Also for the nanopillar-array cell, the V_{oc} was found to increase from 0.55 V at ~20 mW/cm^2 to 0.62 V at ~ 100 mW/cm^2.[38] The much steep slope for the nanowire cell suggests a very different mechanism at work and with potential advantages.

It is generally agreed that a material with a bandgap of about 1.4 eV is the optimal choice for a single-junction solar cell. Based on our theoretical prediction, as revealed in Fig. 5(d), the transition energy between the ZnO core and WZ ZnSe could be as low as 1.5 eV. On this regard, the core/shell nanowires with WZ ZnSe transition layer can very closely match the solar spectrum and in the mean time be chemically more stable than those using a smaller bandgap material as a "sensitizer". Even with an effective bandgap of 1.6 eV, the detailed balance efficiency (Shockley-Queisser) limit of solar cell based on this material would be as high as 29%. This work demonstrates the feasibility of fabricating a high-efficiency solar cell using type-II core/shell nanowires with wide bandgap semiconductors, first suggested in ref. 14. However, there are a number of obstacles to be overcome in order for this approach to realize its full potential. For instance, it is known that making good contacts between coaxial nanowires and electrodes is a big challenge,[38] and in our device, the device resistance is relatively large resulting in a relatively small short-circuit current. Further effort, such as improvement in the Ohmic contact, structural optimization, and device integration, is needed for this new technology to be competitive with the other more mature ones.

4. Conclusions

In this work, we have presented a two-step chemical vapor deposition method for achieving the growth of type-II well-aligned ZnO/ZnSe core/shell nanowire array on a large-area quartz glass substrate. Morphology studies by SEM show that ZnO nanowires with moderate density were grown vertically on the ZnO film substrate and a ZnSe layer was deposited over the entire ZnO nanowire. XRD patterns show strong WZ ZnO (002) and ZB ZnSe (111) peaks, demonstrating the good crystal quality for both the core and shell. TEM images and EDS profiles reveal that the ZnSe transition layer grew coherently on ZnO lateral plane. In the transmission and PL spectra, interfacial transitions between the ZnO core and WZ or ZB ZnSe layer were observed, extending the absorption spectrum well below the ZnSe bandgap into near infrared. For the photovoltaic device based on such a ZnO/ZnSe core/shell NWA, the strong photoresponse associated with the type-II interfacial transition exhibits a threshold of 1.6 eV, which corresponds to an efficiency limit of 29% under one-sun. This work demonstrates the feasibility and great potential for exploring all-inorganic versions of type-II heterojunction solar cells using wide bandgap semiconductors.

Acknowledgements

The work at Xiamen University was supported by "973" Program (2011CB925600), the National Natural Science Foundations of China (60827004, 90921002, and 11044001), the Natural Science Foundations of Fujian Province (A0810019, 2009J01267, and 2010J01343), and the Science and Technology Programs of Fujian Province and Xiamen City. The work of YZ was partially supported by CRI of UNC-Charlotte.

References

1 N. S. Lewis, *Science*, 2007, **315**, 798.
2 K. L. Chopra, P. D. Paulson and V. Dutta, *Progr. Photovolt.: Res. Appl.*, 2004, **12**, 69.
3 R. R. King, D. C. Law, K. M. Edmondson, C. M. Fetzer, G. S. Kinsey, H. Yoon, D. D. Krut, J. H. Ermer, R. A. Sherif and N. H. Karam, *Adv. OptoElectron.*, 2007, 2007 Article ID 29523.
4 M. Grätzel, *Nature*, 2001, **414**, 338.
5 R. Wehrspohn, *ChemSusChem*, 2008, **1**, 173.
6 G. Goncher and R. Solanki, *Proc. SPIE–Int. Soc. Opt. Eng.*, 2008, **7047**, 70470L.
7 K. S. Leschkies, R. Divakar, J. Basu, E. Enache-Pommer, J. E. Boercker, C. B. Carter, U. R. Kortshagen, D. J. Norris and E. S. Aydil, *Nano Lett.*, 2007, **7**, 1793.
8 A. P. Goodey, S. M. Eichfeld, K. K. Lew, J. M. Redwing and T. E. Mallouk, *J. Am. Chem. Soc.*, 2007, **129**, 12344.
9 C. Lévy-Clément, R. T. Zaera, M. A. Ryan, A. Katty and G. Hodes, *Adv. Mater.*, 2005, **17**, 1512.
10 Y. Zhang, J. Pern, A. Mascarenhas and W. L. Zhou, *SPIE Newsroom*, 2008, DOI: 10.1117/2.1200811.1388.
11 Y. J. Lee, D. S. Ruby, D. W. Peters, B. B. McKenzie and J. W. P. Hsu, *Nano Lett.*, 2008, **8**, 1501.
12 L. Hu and G. Chen, *Nano Lett.*, 2007, **7**, 3249.
13 B. M. Kayes, H. A. Atwater and N. S. Lewis, *J. Appl. Phys.*, 2005, **97**, 114302.
14 Y. Zhang, L. Wang and A. Mascarenhas, *Nano Lett.*, 2007, **7**, 1264.
15 A. Nduwimana and X. Q. Wang, *Nano Lett.*, 2009, **9**, 283.
16 J. Schrier, D. O. Demchenko and L. W. Wang, *Nano Lett.*, 2007, **7**, 2377.
17 B. Z. Tian, X. L. Zheng, T. J. Kempa, Y. Fang, N. F. Yu, G. H. Yu, J. L. Huang and C. M. Lieber, *Nature*, 2007, **449**, 885.
18 J. A. Czaban, D. A. Thompson and R. R. LaPierre, *Nano Lett.*, 2009, **9**, 148.
19 Y. J. Dong, B. Z. Tian, T. J. Kempa and C. M. Lieber, *Nano Lett.*, 2009, **9**, 2183.
20 Y. Tak, S. J. Hong, J. S. Lee and K. Yong, *J. Mater. Chem.*, 2009, **19**, 5945.
21 Y. W. Tang, X. Y. Hu, M. J. Chen, L. J. Luo, B. H. Li and L. Z. Zhang, *Electrochim. Acta*, 2009, **54**, 2742.

22 K. Wang, J. J. Chen, W. L. Zhou, Y. Zhang, Y. F. Yan, J. Pern and A. Mascarenhas, *Adv. Mater.*, 2008, **20**, 3248.
23 H. Y. Chao, J. H. Cheng, J. Y. Lu, Y. H. Chang, C. L. Cheng and Y. F. Chen, *Superlattices Microstruct.*, 2010, **47**, 160.
24 E. Janik, A. Wachnicka, E. Guziewicz, M. Godlewski, S. Kret, W. Zaleszczyk, E. Dynowska, A. Presz, G. Karczewski and T. Wojtowicz, *Nanotechnology*, 2010, **21**, 015302.
25 P. Chen, L. Gu and X. B. Cao, *CrystEngComm*, 2010, **12**, 3950.
26 X. D. Wang, C. J. Summers and Z. L. Wang, *Nano Lett.*, 2004, **4**, 423.
27 S. C. Lyu, Y. Zhang and C. Lee, *Chem. Mater.*, 2003, **15**, 3294.
28 K. Wang, J. J. Chen, Z. M. Zeng, J. Tarr, W. L. Zhou, Y. Zhang, Y. F. Yan, C. S. Jiang, J. Pern and A. Mascarenhas, *Appl. Phys. Lett.*, 2010, **96**, 123105.
29 B. Q. Cao, J. Z. Pérez, N. Boukos, C. Czekalla, H. Hilmer, J. Lenzner, A. Travlos, M. Lorenz and M. Grundmann, *Nanotechnology*, 2009, **20**, 305701.
30 J. W. Evans, D. E. Sanders, P. A. Thiel and A. E. DePristo, *Phys. Rev. B: Condens. Matter*, 1990, **41**, 5410.
31 G. Kresse and J. F. Muller, *Phys. Rev. B: Condens. Matter*, 1996, **54**, 11169.
32 S. P. Anthony, J. I. Lee and J. K. Kim, *Appl. Phys. Lett.*, 2007, **90**, 103107.
33 P. Hohenberg and W. Kohn, *Phys. Rev.*, 1964, **136**, B864.
34 Y. H. Li, A. Walsh, S. Y. Chen, W. J. Yin, J. H. Yang, J. B. Li, J. L. F. D. Silva, X. G. Gong and S. H. Wei, *Appl. Phys. Lett.*, 2009, **94**, 212019.
35 Y. Jiang, X. M. Meng, W. C. Yiu, J. Liu, J. X. Ding and C. S. Lee, *J. Phys. Chem. B*, 2004, **108**, 2784.
36 B. Panigrahy, M. Aslam, D. S. Misra, M. Ghosh and D. Bahadur, *Adv. Funct. Mater.*, 2010, **20**, 1161.
37 S. A. Ivanov, A. Piryatinski, J. Nanda, S. Tretiak, K. R. Zavadil, W. O. Wallace, D. Werder and V. I. Klimov, *J. Am. Chem. Soc.*, 2007, **129**, 11708.
38 Z. Y. Fan, H. Razavi, J. Do, A. Moriwaki, O. Ergen, Y. L. Chueh, Paul W. Leu, J. C. Ho, T. Takahashi, L. A. Reichertz, S. Neale, K. Yu, M. Wu, J. W. Ager and A. Javey, *Nat. Mater.*, 2009, **8**, 648.

